

To appear on the Proceedings of the 13th ICATPP Conference on
 Astroparticle, Particle, Space Physics and Detectors
 for Physics Applications,
 Villa Olmo (Como, Italy), 3–7 October, 2011,
 to be published by World Scientific (Singapore).

ELECTRICAL CHARACTERIZATION OF SiPM AS A FUNCTION OF TEST FREQUENCY AND TEMPERATURE

M.J. Boschini^{1,3}, C. Consolandi¹, P.G. Fallica⁴, M. Gervasi^{1,2}, D. Grandi¹,
 M. Mazzillo⁴, S. Pensotti^{1,2}, P.G. Rancoita¹, D. Sanfilippo⁴,
 M. Tacconi^{1*} and G. Valvo⁴

¹*Istituto Nazionale di Fisica Nucleare, INFN Milano-Bicocca, Milano (Italy)*

²*Department of Physics, University of Milano Bicocca, Milano (Italy)*

³*CILEA, Segrate (MI) (Italy)*

⁴*STMicroelectronics, Catania (Italy)*

E-mail: mauro.tacconi@mib.infn.it

Silicon Photomultipliers (SiPM) represent a promising alternative to classical photomultipliers, for instance, for the detection of photons in high energy physics and medical physics. In the present work, electrical characterizations of test devices - manufactured by ST Microelectronics - are presented. SiPMs with an area of $3.5 \times 3.5 \text{ mm}^2$ and a cell pitch of $54 \mu\text{m}$ were manufactured as arrays of 64×64 cells and exhibiting a fill factor of 31%. The capacitance of SiPMs was measured as a function of reverse bias voltage at frequencies ranging from 100 Hz up to 1 MHz and temperatures from 300 K down to 85 K. While leakage currents were measured at temperatures from 400 K down to 85 K. Thus, the threshold voltage - i.e., voltage corresponding to that at which the multiplication regime for the leakage current begins - could be determined as a function of temperature. Finally, an electrical model suited to reproduce the dependence of the frequency dependence of capacitance is presented.

1. Introduction

In recent years Silicon Photomultipliers (SiPM) has been developed for usage in photon detection. The high gain, insensitivity to magnetic field and low reverse bias voltage of operation make SiPM a promising candidates to take the place of classical photomultipliers¹ in several of their applications. The SiPM is an array of parallel-connected single photon avalanche photodiodes (SPAD)². Every SPAD operates in Geiger mode with a quenching resistor in series to prevent an avalanche multiplication

process from taking place. The overall output of a SiPM depends on how many SPADs are simultaneously ignited^{3,4}.

The current SiPM device, manufactured by STMicroelectronics, consists of an array of 64×64 SPAD cells with $3.5 \times 3.5 \text{ mm}^2$ effective area, a cell pitch of $54 \mu\text{m}$ and a fill factor of $\approx 31\%$.

In the present article, the electrical characteristics of these devices are shown as function of the test frequency from 1 MHz down to 10 kHz and temperature from 400 K down 85 K (Sects. 1.1–1.3). In addition, in Sects. 2 and 2.1 an electrical model is discussed and compared with data obtained from dependencies of capacitance and resistance on the test frequency for both a photodiode and a SiPM devices.

1.1. Electrical Characteristics of SiPM Devices

The electrical characteristics of SiPM devices were investigated as function of applied reverse bias voltage (V_r) and temperature. The capacitance response was also studied as a function of the test frequency of the capacimeter employed for such a measurement (Sect. 1.2).

Furthermore (Sect. 1.3), the measurements of the SiPM leakage current allowed one to determine (as a function of the temperature) the value (and its temperature dependence) of the so-called *threshold voltage* (V_{th}), i.e., the reverse bias voltage above which a SiPM begins to operate in Geiger mode.

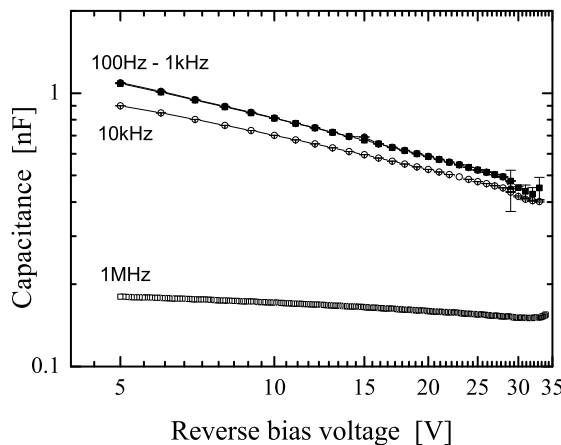


Fig. 1. Capacitance (in nF) as a function of reversed bias voltage (in V) using the LCZ meter with test frequencies of 100 Hz (●), 1 kHz (■), 10 kHz (○) and BC with 1 MHz (□).

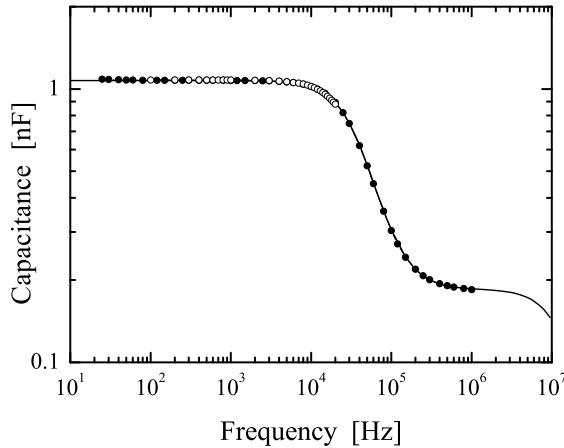


Fig. 2. Capacitance (in nF) as a function of the test frequency (in Hz) for a sample operated with a reverse bias of 5 V: data points indicated with \bullet (\circ) were obtained using the LCR (LCZ) meter, the continuous line is obtained from Eq. (9) (see discussion in Sect. 2.1).

1.2. Capacitance Response

The capacitance response of SiPM devices was systematically measured as a function of the reverse bias voltage applied and test frequency at 290 K. In addition, using a liquid nitrogen cryostat, at a few fixed frequencies the capacitance was also measured as a function of the reverse bias voltage and temperature from 300 K down to 85 K. For these purposes three instruments were employed, i.e., a Boonton capacimeter (BC) (using its internally provided power source and a test frequency of 1 MHz), an LCZ (Agilent Technologies 4276A) and LCR (Agilent Technologies 4284A) meters with the reverse bias supplied to the device from an external power supply. The LCZ meter employed test frequencies from 100 Hz up to 20 KHz; the LCR meter from \approx 20 Hz up to 1 MHz. Furthermore, the measurements were performed selecting the parallel equivalent-circuit mode of the LCR and LCZ meters for the device under test (DUT). Thus, the device response is assumed to be that one from a parallel capacitor-resistor circuit (see discussion in Sect. 2). Finally, the currently reported experimental errors are the standard deviations obtained using 50 subsequent measurements of the device capacitance under the same experimental conditions.

In Fig. 1, the capacitance response using frequencies of 100 Hz, 1 kHz, 10 kHz and 1 MHz of a SiPM is shown as a function of V_r at 290 K. Above

1 kHz, the measured capacitance decreases with increasing the test frequency. In Fig. 2, the capacitance response - determined using both LCZ and LCR meters - is shown for a device operated with a reverse bias voltage of 5 V at 290 K. It can be observed that above ≈ 10 kHz the measured capacitance largely decreases with increasing the test frequency of the instrument up to reaching an almost constant response above a few hundreds of kHz.

In Fig. 3, the capacitance response using 100 Hz, 1 kHz, 10 kHz and 1 MHz is shown as a function of V_r (in V) and temperature from 300 K down to 85 K. The measured capacitance is observed to decrease with decreasing temperature. This behavior is also observed for frequencies lower than ≈ 10 kHz; while a similar capacitance response was exhibited at 290 K (see Fig. 1).

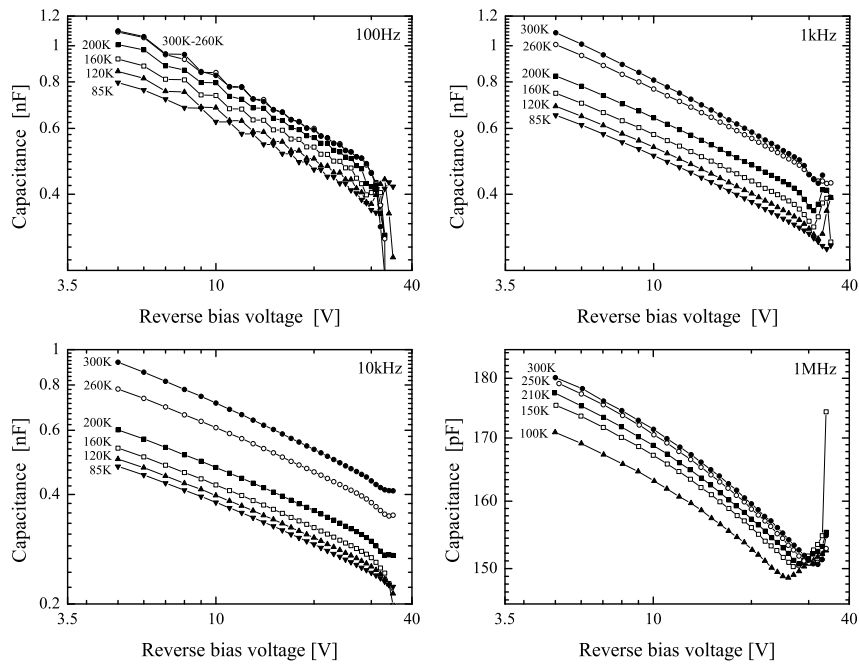


Fig. 3. Capacitance response (in nF or pF) obtained using the LCZ meter as a function of the reverse bias applied (in V) and temperature from 300 K down to 85 K: 100 Hz (upper left), 1 kHz (upper right), 10 kHz (bottom left) and - using the BC - 1 MHz (bottom right).

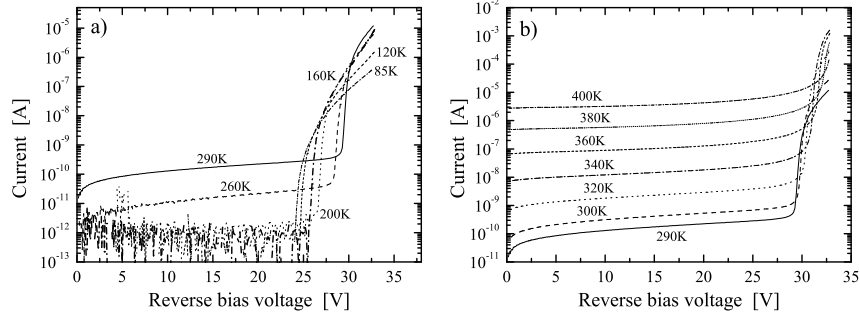


Fig. 4. (a) Leakage current (in A) as a function of reverse bias voltage (in V) from 300 down to 85 K; (b) leakage current (in A) as a function of reverse bias voltage (in V) from 290 up to 400 K.

1.3. Current-Voltage Characteristics

The dependence of leakage current on reverse bias was determined as a function of the temperature from 400 K down to 85 K and is shown in Fig. 4. With increasing V_r the leakage current does not vary by more than an order of magnitude until the multiplication regime is ignited, i.e., so far the *threshold voltage*, V_{th} , is reached. V_{th} is the voltage corresponding to the value of leakage current at the interception between the two I versus V curves obtained the first when the multiplication regime is sharply starting and the second one at lower voltages, i.e., before the multiplication occurs: an example regarding the determination of the value of V_{th} at 260 K is reported in Fig. 5(a). As shown in Fig. 5(b), the threshold voltage lowers - thus, SPADs turn into a Geiger-mod regime at progressively lower reverse

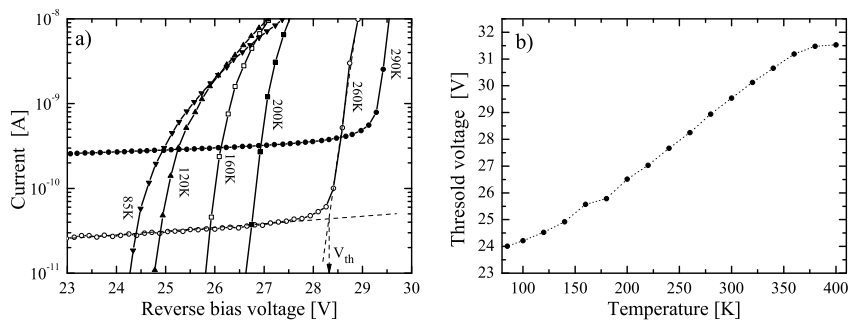


Fig. 5. (a) Leakage current (in A) as a function of the reverse bias voltage applied (in V) and an example of threshold voltage, V_{th} in V, determination at 260 K; (b) threshold voltage (in V) as a function of temperature (in K).

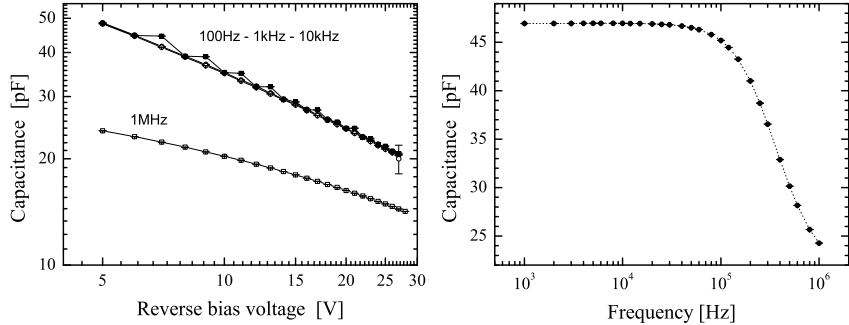


Fig. 6. (a) Capacitance (in pF) of a photodiode as a function of the reverse bias voltage (in V) at 100 Hz, 1 kHz, 10 kHz (using the LCZ meter) and 1 MHz (using the BC); (b) capacitance (in pF) of a photodiode as a function of the test frequency in Hz (using the LCR meter) with an applied reverse biased voltage of 6 V.

bias voltages - with lowering temperature at the rate of $\approx -29 \text{ mV/K}$ from 290 down to 85 K.

2. Electrical Model

The electrical frequency response of SiPMs was further investigated using a test device manufactured by STMicroelectronics. The latter device was a photodiode (PD) with a structure similar to that of a SPAD cell, an active area of $\approx 0.2 \text{ mm}^2$, but no quenching resistor in series. In Fig. 6(a), the capacitance of the PD is shown as a function of the reverse bias voltage at 100 Hz, 1 kHz, 10 kHz and 1 MHz. Furthermore, one can see that the device exhibits almost no dependence of the test frequency below $\approx 100 \text{ kHz}$ [Fig. 6(b)].

For silicon photodiodes and radiation detectors, the electrical response down to cryogenics temperatures are usually modeled using the so-called *small-signal ac impedance of junction diode* (SIJD) operated under reverse bias (e.g., see Refs.^{5,6}, Section 4.3.4 of Ref.⁷ and also references therein). In

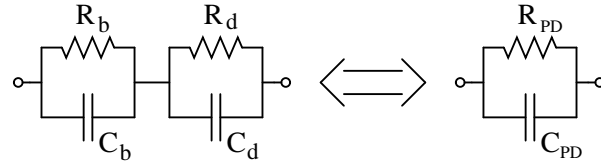


Fig. 7. SIJD model for silicon photodiodes and radiation detectors: C_d (C_b) and R_d (R_b) are the capacitance and resistance of the depleted (field free) region, respectively; C_{PD} and R_{PD} are respectively the overall capacitance and resistance of the photodiode.

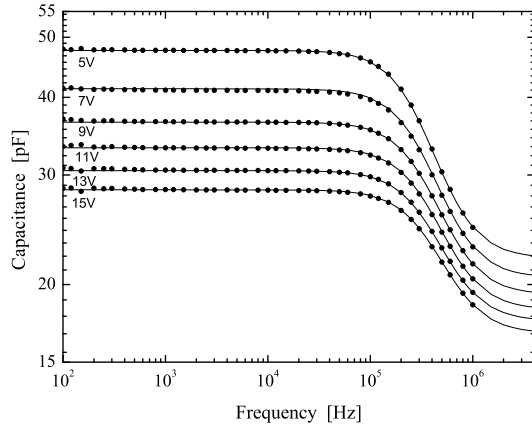


Fig. 8. Measured capacitance (\bullet), C_{PD} , in pF as a function of the test frequency in Hz with over-imposed continuous lines obtained from the SIJD model [Eq. (3)].

the framework of the SIJD model, the device exhibits both depleted and field free regions which are represented as two circuits in series, each one consisting of a parallel-connected circuit of a capacitor and a resistor. In Fig. 7, the equivalent circuit of a photodiode is shown: C_d (C_b) and R_d (R_b) are the capacitance and resistance of the depleted (field free) region, respectively.

Indicating (Fig. 7) the overall capacitance and resistance of a photodiode

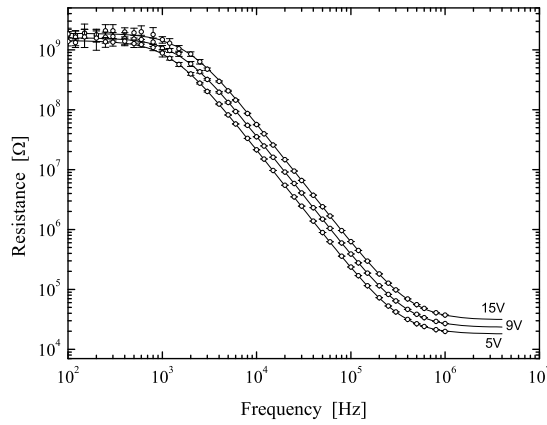


Fig. 9. Measured resistance (\circ), R_{PD} , in Ω as a function of the test frequency in Hz at 5, 9 and 15 V with over-imposed continuous lines obtained from the SIJD model [Eq. (2)].

Table 1. C_d , R_d , C_b and R_b obtained from a fit of the SIJD model for a photodiode to experimental data as a function of reverse bias voltage (V_r).

V_r [V]	C_d [pF]	R_d [GΩ]	C_b [pF]	R_b [kΩ]
5	47.6	1.42	41.1	5.2
7	41.1	1.53	40.8	5.2
9	36.5	1.58	40.8	5.2
11	33.2	1.68	40.4	5.2
13	30.5	1.74	40.9	5.3
15	28.4	1.88	40.5	5.3

with C_{PD} and R_{PD} , respectively, one can express the admittance of the device as:

$$Y_{PD}(\omega) = G_{PD}(\omega) + j B_{PD}(\omega) = \frac{1}{R_{PD}} + j \omega C_{PD} \quad (1)$$

with $\omega = 2\pi f$, f the test frequency. The conductance (i.e., the real part of the admittance) and susceptance (the imaginary part of the admittance) are respectively given by:

$$G_{PD}(\omega) = \frac{1}{R_{PD}} = \frac{R_d + R_b + \omega^2 R_d R_b (R_d C_d^2 + R_b C_b^2)}{(R_d + R_b)^2 + \omega^2 R_d^2 R_b^2 (C_b + C_d)^2} \quad (2)$$

$$B_{PD}(\omega) = \omega C_{PD} = \omega \left[\frac{\omega^2 R_d^2 R_b^2 C_d C_b (C_b + C_d) + R_d^2 C_d + R_b^2 C_b}{(R_d + R_b)^2 + \omega^2 R_d^2 R_b^2 (C_b + C_d)^2} \right] \quad (3)$$

[e.g., see Equations (4.184, 4.185) at page 455 of Ref.⁷].

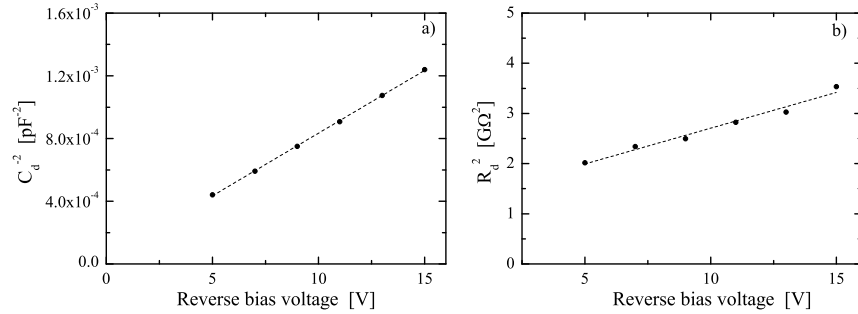


Fig. 10. (a) $1/C_d^2$ in pF^{-2} and (b) R_d^2 in $\text{G}\Omega^2$ from Table 1 as a function of the applied reversed bias voltage in V. The dashed lines are those from a linear fit to data.

It has to be remarked that the values of both C_{PD} and R_{PD} are those which can be determined, for instance, selecting the parallel equivalent-circuit mode for the DUT using the LCR meter. In the SIJD model, the values of C_d , R_d , C_b and R_b do not depend on the test frequency. In addition, C_d , R_d are expected to depend on the applied reverse bias voltage, because the depleted layer width increases with increasing V_r .

C_d , R_d , C_b and R_b were determined (Table 1) as a function V_r , by a fit to the measured quantities C_{PD} and R_{PD} (obtained using the LCR meter) using the corresponding expressions [e.g., see Eqs. (2, 3)] obtained from the SIJD model for a photodiode. For instance, in Fig. 8 (Fig. 9) the experimental data and fitted curves are shown for the capacitance (resistance) measurements as a function of the test frequency and applied reverse bias voltage. As expected⁵ (Table 1), the field free region is almost independent of V_r , while both the capacitance and resistance of the depleted region exhibit a dependence on the reverse bias. In Fig. 10, $1/C_d^2$ [Fig. 10(a)] and R_d^2 [Fig. 10(b)] values from Table 1 are shown as a function of the applied reverse voltage. Although the junction photodiode cannot be considered a one-sided step junction, the dashed curves (Fig. 10) obtained from fits to the reported data - assuming a linear dependence of $1/C_d^2$ and R_d^2 on V_r - are well suited to reproduce the dependence on the reverse bias voltage.

2.1. Electrical Model for SiPMs

A SiPM device consists of a set of SPAD devices (4096 in the current SiPM under test) connected in parallel. The equivalent electrical circuit of the elemental cell (i.e., a SPAD cell) is shown in Fig. 11 and differs from that of a photodiode (discussed in Sect. 2) by a resistance (R_s) added in series. In Fig. 11, C_d (C_b) and R_d (R_b) are the capacitance and resistance of the depleted (field free) region, respectively. In the present technology of STMicroelectronics, R_s is typically about (0.2–1.0) MΩ.

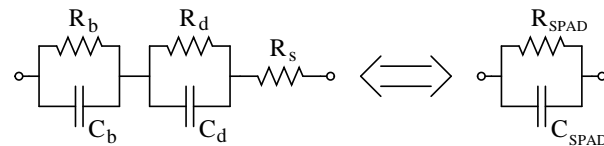


Fig. 11. SIJD model for a SPAD cell: C_d (C_b) and R_d (R_b) are respectively the capacitance and resistance of the depleted (field free) region with R_s a series resistance; C_{spad} and R_{spad} are respectively the overall capacitance and resistance of a SPAD cell.

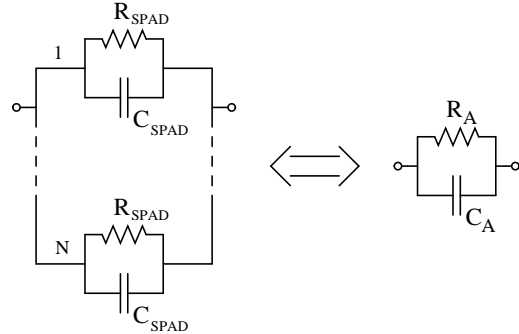


Fig. 12. SIJD model for a SiPM device consisting of N SPAD devices connected in parallel: C_{spad} and R_{spad} are respectively the capacitance and resistance of the equivalent circuit of a SPAD cell (Fig 11), C_A and R_A those of the SiPM device.

The admittance (Y_{spad}) of a SPAD cell is given by

$$\begin{aligned} Y_{\text{spad}}(\omega) &= G_{\text{spad}}(\omega) + j B_{\text{spad}}(\omega) \\ &= \frac{1}{R_{\text{spad}}} + j \omega C_{\text{spad}} \end{aligned} \quad (4)$$

with C_{spad} and R_{spad} respectively expressed in terms of C_d , C_b , R_d , R_b and R_s as

$$\begin{aligned} C_{\text{spad}} &= \frac{B_{\text{spad}}(\omega)}{\omega} \\ &= \frac{\omega^2 R_d^2 R_b^2 C_d C_b (C_b + C_d) + R_d^2 C_d + R_b^2 C_b}{D_1 + D_2}, \end{aligned} \quad (5)$$

$$\begin{aligned} R_{\text{spad}} &= \frac{1}{G_{\text{spad}}(\omega)} \\ &= \frac{D_1 + D_2}{R_b + (1 + \omega^2 C_b^2 R_b^2)(R_s + R_d) + \omega^2 R_d^2 C_d^2 (\omega^2 C_b^2 R_s R_b^2 + R_s + R_b)}, \end{aligned} \quad (6)$$

where D_1 and D_2 are

$$\begin{aligned} D_1 &= \omega^2 R_b^2 C_b^2 (R_s + R_d)^2 + \omega^2 R_d^2 C_d^2 (R_s + R_b)^2 \\ D_2 &= (R_d + R_b + R_s)^2 + \omega^2 R_d^2 R_b^2 C_d C_b (2 + \omega^2 R_s^2 C_d C_b). \end{aligned}$$

The equivalent electrical circuit* of a SiPM is shown in Fig. 12. Assuming that each SPAD cell has the same admittance, one finds that the overall

*It has to be remarked that one can also add a series resistance to R_A . This was the case for another SiPM device with 3600 SPAD cells manufactured by STMicroelectronics: for such a device a small additional series resistance of about $1\text{k}\Omega$ was needed.

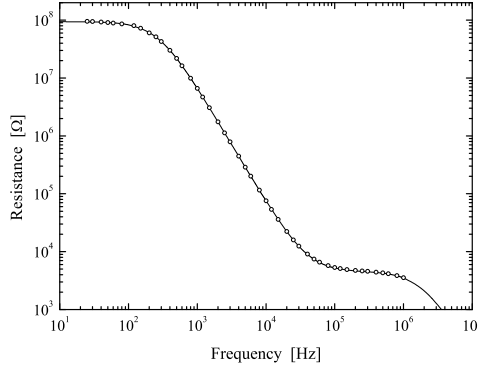


Fig. 13. Measured resistance (o), R_A , in Ω as a function of the frequency in Hz with over-imposed the continuous lines obtained from Eq. (8).

admittance of an array is determined by:

$$\begin{aligned}
 Y_A(\omega) &= N Y_{\text{spad}}(\omega) \\
 &= G_A(\omega) + j B_A(\omega) \\
 &= \frac{1}{R_A} + j \omega C_A
 \end{aligned} \tag{7}$$

with

$$G_A(\omega) = \frac{N}{R_{\text{spad}}} \tag{8}$$

$$B_A(\omega) = \omega N C_{\text{spad}}, \tag{9}$$

C_{spad} and R_{spad} from Eqs. (5, 6), respectively; finally, $N = 64 \times 64 = 4096$ for the present device.

Table 2. C_d , R_d , C_b , R_b and R_s obtained from a fit of the SIJD model (adapted to a SiPM) to experimental data with the device operated at a reverse bias voltage of 5 V.

V_r [V]	C_d [pF]	R_d [GΩ]	C_b [pF]	R_b [MΩ]	R_s [kΩ]
5	0.262	385	0.056	12.5	195

In Fig. 2 (13), the measured values of the capacitance (resistance) - obtained using the LCR meter with the SiPM device operated at a reverse bias

voltage of 5 V - are shown as a function of the test frequency up to 1 MHz, while the continuous line is that obtained using Eq. (9) [Eq. (8)]. Finally, in Table 2 the values of C_d , R_d , C_b , R_b and R_s obtained from such a fit of the SIJD model (adapted to a SiPM) to experimental data are reported. It can be remarked that the obtained value of R_s is in agreement with one of those typically used in the current technology.

3. Conclusions

The electrical characteristics of SiPM devices were investigated as a function of the applied reverse bias voltage (V_r) and temperature from 400 down to 85 K. The capacitance response was also studied as a function of the test frequency. One finds that the measured capacitance decreases i) with increasing the test frequency above 10 kHz at 290 K and ii) with decreasing the temperature.

Furthermore), the measurement of the leakage current allowed one to determine the value (and its temperature dependence) of the threshold voltage (V_{th}) above which a SiPM begins to operate in Geiger mode: V_{th} decreases with lowering temperature at the rate of ≈ -29 mV/K from 290 down to 85 K.

It was developed an electrical model to treat the frequency dependence of a SiPM device operated under reverse bias voltage based on the so-called small-signal ac impedance of junction diode (SIJD) used for radiation detectors and photodiodes. The model was found to be well suited to account for the SiPM dependencies of capacitance and resistance on frequency.

References

1. V.D. Kovaltchouk et al., *Nucl. Instr. and Meth. in Phys. Res. A* 538 (2005), 408–415.
2. M. Mazzillo et al., *Nucl. Instr. and Meth. in Phys. Res. A* 591 (2008), 367–373.
3. F. Zappa et al., *Sens. Actuat. A* 140 (2007), 103–112.
4. M. Mazzillo et al., *Sens. Actuat. A* 138 (2007), 306–312.
5. C.H. Champness, *J. of App. Phys.* 62 (1987), 917.
6. C. Leroy and P.G. Rancoita, Particle Interaction and Displacement Damage in Silicon Devices operated in Radiation Environments, *Rep. Prog. in Phys.* 70 (2007), 403–625, doi: 10.1088/0034-4885/70/4/R01.
7. C. Leroy and P.G. Rancoita, Principles of Radiation Interaction in Matter and Detection - 3rd Edition - (2011), World Scientific, Singapore, ISBN-978-981-4360-51-7.